
DEEP LEARNING TECHNIQUES FOR BLIND IMAGE SUPER-RESOLUTION: A HIGH-SCALE MULTI-DOMAIN PERSPECTIVE EVALUATION

Valdivino Alexandre de Santiago Júnior

Coordenação de Pesquisa Aplicada e Desenvolvimento Tecnológico (COPDT)

Instituto Nacional de Pesquisas Espaciais (INPE)

São José dos Campos, São Paulo, Brazil

valdivino.santiago@inpe.br

ABSTRACT

Despite several solutions and experiments have been conducted recently addressing image super-resolution (SR), boosted by deep learning (DL) techniques, they do not usually design evaluations with high scaling factors, capping it at 2x or 4x. Moreover, the datasets are generally benchmarks which do not truly encompass significant diversity of domains to properly evaluate the techniques. It is also interesting to remark that blind SR is attractive for real-world scenarios since it is based on the idea that the degradation process is unknown, and hence techniques in this context rely basically on low-resolution (LR) images. In this article, we present a high-scale (8x) controlled experiment which evaluates five recent DL techniques tailored for blind image SR: Adaptive Pseudo Augmentation (APA), Blind Image SR with Spatially Variant Degradations (BlindSR), Deep Alternating Network (DAN), FastGAN, and Mixture of Experts Super-Resolution (MoESR). We consider 14 small datasets from five different broader domains which are: aerial, fauna, flora, medical, and satellite. Another distinctive characteristic of our evaluation is that some of the DL approaches were designed for single-image SR but others not. Two no-reference metrics were selected, being the classical natural image quality evaluator (NIQE) and the recent transformer-based multi-dimension attention network for no-reference image quality assessment (MANIQA) score, to assess the techniques. Overall, MoESR can be regarded as the best solution although the perceptual quality of the created HR images of all the techniques still needs to improve. We believe that independent and unbiased evaluations, like this one, are important to indicate the most suitable approaches to be selected by professionals who need to work with image SR in their practical settings. Supporting code: https://github.com/vsantjr/DL_BlindSR. Datasets: <https://www.kaggle.com/datasets/valdivinosantiago/dl-blindsr-datasets>.

Keywords Image super-resolution · Artificial intelligence · Deep learning · Controlled experiment · Multiple domains

1 Introduction

Medical imaging [1, 2, 3, 4], internet video delivery [5, 6, 7], surveillance and security via person identification [8, 9, 10], and remote sensing [11, 12, 13, 14, 15, 16] are just some examples of real-world applications where image super-resolution (SR) has been used. In SR, we aim at recovering high-resolution¹ (HR) images from low-resolution (LR) ones. This is a non-trivial and generally ill-posed problem since multiple HR images exist corresponding to a unique LR image [17].

Several classical methods have been designed for image SR such as bicubic interpolation and Lanczos resampling [18], edge-based methods [19], statistical methods [20], among others. But, naturally, with all the developments related to

¹In this article, image resolution means precisely the dimensionality of the image. For instance, an image has a resolution of $W \times H$ pixels. This is not to be confused with other definitions of resolution existing in certain communities such as remote sensing (spatial resolution, radiometric resolution, temporal resolution, ...).

deep learning (DL) and deep neural networks (DNNs) [21], a significant number of strategies have been proposed addressing SR via DL/DNNs as reported in recent secondary studies [17, 11]. Among the DL techniques, convolutional neural networks (CNNs) [22, 23, 24, 13], generative adversarial networks (GAN) [25, 26, 12, 14], and attention-based networks [27, 28, 15] have been employed to solve image SR problems.

The majority of studies published up to now focus on supervised SR where models are trained with both LR images and the corresponding HR ones [17, 11]. But, in reality, it is not easy to have images from the same scene but with distinct resolutions so that having the pairs LR-HR for training is not as direct as it is supposed to be. Hence, in unsupervised SR [29], only unpaired LR-HR images are available for training, so that the models are more able to learn real-world LR-HR mappings.

But an even more attractive strategy for real-world scenarios is blind image SR [30, 31] which is based on the idea that the degradation process/kernels is/are unknown, and hence techniques in this context rely basically on LR images, not requiring the high-resolution ones. There is an increasing interest in blind image SR.

Despite the huge number of proposed techniques and experiments boosted by DL techniques [17, 11], they do not usually design evaluations with high scaling factors, capping it at 2x or 4x. One of the exceptions is the experiment presented in [11] where authors considered 2x, 4x, and 8x scaling factors. However, the authors considered a multi-sensor remote sensing dataset (MSRSD) consisting of mostly publicly available very HR satellite images. Even if the images are from different satellites and regions, eventually the diversity of the images and feature spaces are not enough to properly evaluate SR techniques.

Several other datasets have been used for training image SR approaches such as BSDS300 [32], BSDS500 [33], DIV2K [34], PIRM [35], Set5 [36], Set14 [37], and Urban100 [38]. These datasets comprise different categories but still lack of images of other domains. For instance, all the datasets above do not seem to present images obtained via satellite sensors or medical images. Interesting to stress that images taken by sensors embedded in satellites or airplanes have considerable differences compared to natural images due to different shooting content and shooting methods [39]. Moreover, as previously remarked, evaluations are usually limited to the 4x scaling factor. In [40], results are presented for 8x scaling factor but considering only the Set5 and Set14 datasets. We believe that performing experiments addressing not only high scaling factors (e.g. 8x) but also datasets of different domains is very important to better identify the most adequate image SR approaches.

Image quality assessment (IQA) metrics (methods) are roughly divided into two categories: full-reference (FR-IQA) and no-reference (NR-IQA) [41]. In FR-IQA, we evaluate the similarity between a distorted image and a given reference image, and classical metrics which have been extensively used are peak signal-to-noise ratio (PSNR) [11] and structural similarity index measure (SSIM) [42]. On the other hand, NR-IQA metrics are proposed to assess image quality without a reference image, being more suitable for perceptual quality. Natural image quality evaluator (NIQE) [43] and perception index (PI) [35] are two traditional metrics. However, recent metrics can be devised based on DNNs as presented in the **New Trends in Image Restoration and Enhancement** (NTIRE) workshop held at CVPR 2022 [41]. And, for the first time, NTIRE 2022 Challenge on Perceptual Image Quality Assessment had a track addressing NR-IQA. We believe that for evaluating approaches in a completely “blind” setting, NR-IQA metrics are more interesting since they do not demand a reference image, only the LR ones.

In this article, we present a high-scale (8x) controlled experiment which evaluates five recent DL techniques tailored for blind image SR: Adaptive Pseudo Augmentation (APA) [44], Blind Image SR with Spatially Variant Degradations (BlindSR) [45], Deep Alternating Network (DAN) [46], FastGAN [47], and Mixture of Experts Super-Resolution (MoESR) [48]. Relying basically on public sources, we adapt and create 14 small (100 samples) LR images datasets from five different broader domains: aerial, fauna, flora, medical, and satellite². Another distinctive characteristic of our evaluation is that some of the DL approaches were designed for single-image SR but others not.

Two NR-IQA metrics were selected, being the classical NIQE and the recent vision transformer(ViT)-based multi-dimension attention network for no-reference image quality assessment (MANIQA) score [49], to assess the techniques. The MANIQA model was the winner of the NTIRE 2022’s NR-IQA track obtaining a performance considerably higher than classical strategies such as PI and NIQE.

The contributions of this study are:

1. We design and execute a controlled experiment considering five recent blind image SR approaches and focusing on a specific large scaling factor (8x). Note that we decided to present a more detailed analysis of the results,

²The aerial broader domain means data/images obtained at altitudes lower than 100 km (62 miles; Kármán Line) above the mean sea level. For example, images obtained by sensors attached/embedded in airplanes or unmanned aerial vehicles (drones). The satellite broader domain relates to the space and it implies data/images obtained from sensors, usually onboard satellites, which are at a minimum altitude of 100 km above the mean sea level.

trying to explain in more depth the behaviours of the approaches. We also perform a correlation analysis taking into account the HR images produced by the two best DL techniques. We believe that independent and unbiased evaluations are important to indicate the most suitable approaches to be selected by professionals who need to work with image SR in their practical settings;

2. We adapt and create 14 small (100 samples) LR images datasets from five different broader domains: aerial, fauna, flora, medical, and satellite. We believe that making available these small datasets to the community, obtained from quite distinct domains, is interesting to provide other possibilities to evaluate the blind image SR techniques considering not only single-image but non-single-image techniques (we had indeed done this);
3. We consider a recent DNN-based NR-IQA metric (MANIQA score) in addition to a classical one (NIQE), and present some remarks by using such metrics.

This article is structured as follows. Section 2 briefly presents the theoretical background and related work. In Section 3, we show in detail the design of our experiment. Results are in Section 4 while Section 5 discusses some important points. In Section 6, conclusions and feature directions are pointed out.

2 Background

This section presents an overview of the theoretical background related to image SR. More details can be seen elsewhere [17, 11]. At the end, we also discuss about related work. The goal of image SR is to recover the corresponding HR images from the LR images. The LR image, I_{LR} , is usually modelled as the output of the following degradation:

$$I_{LR} = \Gamma(I_{HR}; \delta) \quad (1)$$

where Γ means a degradation mapping function, I_{HR} is the corresponding HR image, and δ represents the parameters of the degradation process. When the degradation process (Γ and δ) is unknown, which is very common to happen, and only LR images are available for the techniques, we have the so called blind image SR. In this case, the idea is to recover an HR approximation, \widehat{I}_{HR} , of the ground truth HR image, I_{HR} , from the LR image as presented below:

$$\widehat{I}_{HR} = \mathcal{M}(I_{LR}; \theta) \quad (2)$$

where \mathcal{M} is the SR model and θ are the parameters of \mathcal{M} .

Despite of the fact that the degradation process is usually unknown, several studies model the degradation as follows:

$$\Gamma(I_{HR}; \delta) = (I_{HR}) \downarrow s, \{s\} \subset \delta \quad (3)$$

where \downarrow is a downsampling operation and s is a scaling factor. But, some studies [50] do such a degradation modelling as presented below:

$$\Gamma(I_{HR}; \delta) = (I_{HR} \otimes \kappa) \downarrow s + \varphi_\xi, \{\kappa, s, \xi\} \subset \delta \quad (4)$$

where $I_{HR} \otimes \kappa$ means the convolution between a blur kernel, κ , and the HR image, I_{HR} , and s is a scaling factor. Moreover, φ_ξ is some additive white Gaussian noise with standard deviation ξ .

2.1 Metrics

As previously mentioned, there are several metrics for IQA, being full-reference (FR-IQA) or without relying on a reference (NR-IQA). We present here a brief discussion about the two NR-IQA metrics we have considered in this research: NIQE [43] and MANIQA score [49].

The main motivation to develop NIQE is that, at the time it was proposed, NR-IQA models required knowledge about anticipated distortions in the form of training samples and corresponding human opinion scores. Thus, NIQE is a completely blind approach which only uses measurable deviations from statistical regularities observed in natural images, without training on human-rated distorted images and, hence, without any exposure to distorted images. The idea is to construct a “quality aware” collection of statistical features based on a successful space domain natural scene statistic (NSS) model.

NIQE is derived by computing 36 identical NSS features from patches of the same size, $P \times P$, from the image to be analysed, fitting them with a multivariate Gaussian model (MVG) [51], then comparing its MVG fit to the natural MVG model. They considered a patch of dimension (resolution) 96×96 , although other dimensions were also evaluated. The quality of the distorted image is expressed as the distance between the quality aware NSS feature model and the MVG fit to the features extracted from the distorted image, as shown below:

$$\mathcal{D}(\nu_1, \nu_2, \Sigma_1, \Sigma_2) = \sqrt{\left((\nu_1 - \nu_2)^T \left(\frac{\Sigma_1 + \Sigma_2}{2} \right)^{-1} (\nu_1 - \nu_2) \right)} \quad (5)$$

where ν_1 and ν_2 are the mean vectors of the natural MVG model and the distorted image's MVG model, respectively. Furthermore, Σ_1 and Σ_2 are the covariance matrices of the natural MVG model and the distorted image's MVG model, respectively. Thus, as **lower** the NIQE, the better the perceptual quality of the generated HR image.

While NIQE is a very traditional metric, the MANIQA score is a very recent one. Top approach of the NTIRE 2022's NR-IQA track [41], the motivation for the development of the MANIQA model and its corresponding score is that NR-IQA metrics/methods are limited when assessing images created by GAN-based image restoration algorithms [26, 52]. As shown in Fig. 1, the MANIQA model consists of four components: feature extractor using ViT [53], transposed attention block, scale swin transformer block, and a dual-branch structure for patch-weighted quality prediction.

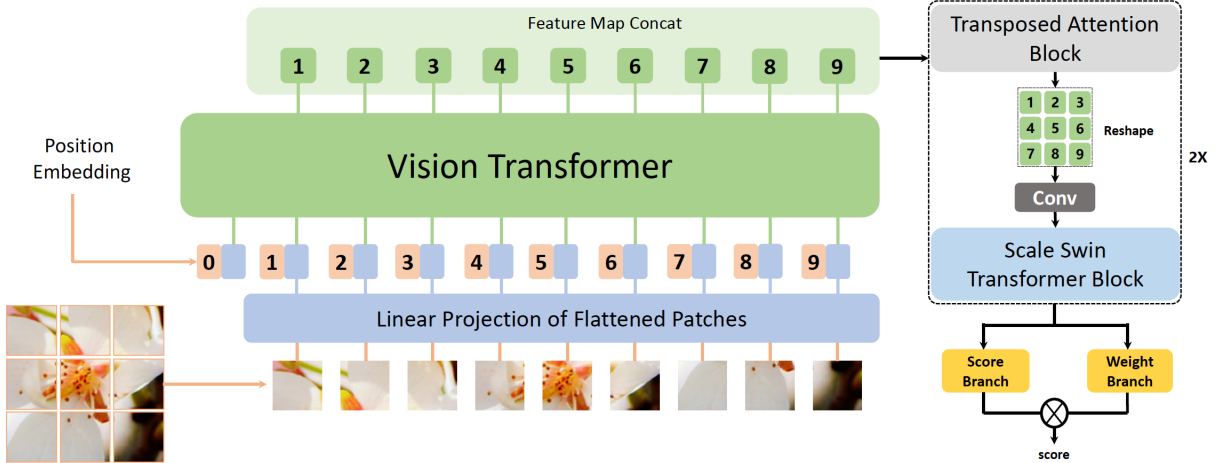


Figure 1: The MANIQA model. The score is the metric related to the image. Source: adapted from [49]

In more detail, a distorted image is cropped into patches of dimension 8×8 . Then, the patches are inputted into the ViT for extracting the features. Transposed attention block and scale swin transformer block are used to strengthen the global and local interaction. A dual-branch structure is proposed for predicting the weight and score of each patch. Notice that as **higher** the MANIQA score, the better the perceptual quality of the generated HR image.

2.2 Related work

This study is an experiment within blind image SR via DL/DNNs. Basically every study within blind image SR presents experimental evaluations and, in lesser or greater extent, they are related to ours. As mentioned in Section 1, even if there are so many techniques and experiments proposed boosted by DL techniques, as corroborated by secondary studies [17, 11], in general the studies do not consider high scaling factors such as 8x. When there are exceptions [11, 40], there is no significant diversity of images and feature spaces to proper evaluate the image SR approaches, taking into account quite distinct broader domains such as medicine images, images obtained by satellites via sensors with different characteristics, and images more "usual" like those of animal's faces.

It is worth noting that dealing with this range of different domains is important to better classify the techniques in terms of their performances. In other words, the wider/general the assessments are, the better. Furthermore, independent evaluations, like the one presented in this article, are valuable to guide professionals in making the correct decisions in

choosing the most appropriate blind image SR solution. Our study addresses all these previous points and these are the main differences between our effort and other already published articles.

3 Experiment design

In this section, we describe the main design options of the controlled experiment to assess the performance of the five DL techniques for blind image SR: APA, BlindSR, DAN, FastGAN, and MoESR.

3.1 Research questions and variables

The research questions (RQs) related to this experiment are:

1. **RQ₁** - Which out of the five algorithms for blind image SR is the best regarding the metrics NIQE and MANIQA score? And which can be considered the best overall?
2. **RQ₂** - Does the two top approaches present similar behaviours when deriving HR images?

The motivation for **RQ₁** is self-explained. Regarding **RQ₂**, the idea here is to perceive whether the two best approaches present similar behaviours. In other words, are the images detected as having the best, as well as the worst, quality perceptions, based on the MANIQA scores, somewhat “common” to both best DL techniques? Our goal here is to see whether the best algorithms “agree” in terms of the HR images they create based only on the LR ones. The independent variables are the DL models. The dependent variables are the values of the metrics, i.e. NIQE and MANIQA score.

3.2 Datasets

The 14 datasets comprise five different broader domains: aerial, fauna, flora, medical, and satellite. Tables 1 and 2 present details about the datasets we created based on publicly released images. In Table 2, note that the original resolution of the images in the datasets are diverse. Some source datasets, like *condoaerial* and *massachbuildings*, are formed by HR images where all samples have the same resolution. The *plantpat* dataset has HR images too but there are several different resolutions. Others like *catsfaces* and *isaid* have HR, LR and even medium resolution images. Three Satellite datasets, *amazonia1*, *cbers4a*, and *deepglobe*, are composed only by LR images and all have the same resolution.

Given the different domains and image resolutions (in some cases, as shown in Table 2, we just had at our disposal LR images), we therefore decided to default the input LR images to a resolution of 128 x 128 pixels. Thus, we downsampled the images which have higher resolution than that based on the bicubic interpolation method as many others have been doing [17, 11]. Fig. 2 presents some LR images from the datasets we created.

Note that some criticise doing such a resizing because real-world cameras actually accomplishes a series of operations (demosaicing, denoising, ...) to finally produce 8-bit RGB images [17]. Thus, RGB images have lost lots of original signals becoming significant different from the original images taken by the camera. Therefore, it would not be interesting to directly use the manually downsampled RGB images by using, for instance, a bicubic interpolation method for image SR.

However, we must emphasise that our main goal is to perform an experiment using DL techniques for blind image SR, based on different domains, in order to provide some sort of recommendation to professionals who need to choose a technique that best fit their needs. Although the issues cited earlier exist, they impact equally all the DL techniques and hence they do not compromise our analysis.

In addition to standardising the resolution of the LR input images, we also considered the same small number of images in the datasets: 100 samples. More details about this point in the next section.

3.3 Amount of required images

Taking into account the “amount” of required images, recent DL techniques for image SR are created assuming a single image, known as single-image SR, but they can also be devised assuming that there are a few (limited) number of samples, which we can call few-shot image SR. There is currently a great interest in few-shot learning (FSL) where we face the situation to solve a task based on few samples with supervised information [54]. Note that here we consider that few-shot SR assumes few but more than one image. There are also other possibilities, like zero-shot SR presented by [55], where authors coped with unsupervised SR by training image-specific SR networks at test time rather than training a model on huge datasets.

Table 1: Datasets: description and source

Domain	Dataset	Description	Source
Aerial	condoaerial	Aerial Semantic Segmentation Drone Dataset	https://bit.ly/3YWXNYy
	massachbuildings	Massachusetts Buildings Dataset	https://bit.ly/41nS4fI
	ships	Ship Detection from Aerial Images Dataset	https://bit.ly/3ZaPEiK
	ufsm-flame	Drone Images from UFSM and Flame Datasets	https://bit.ly/3KxJzbZ https://bit.ly/3YUwA8B https://bit.ly/3ZhiSMZ
Fauna	catsfaces dogsfaces	Cats Faces Dataset Dogs Faces Dataset	https://bit.ly/41gDrLv https://bit.ly/41gDrLv
Flora	flowers	102 Category Flower Dataset	https://bit.ly/3EAxH5w
	plantpat	Plant Pathology 2021 - FGVC8 - Dataset	https://bit.ly/3EBCkMv
Medical	melanomaisic	SIIM-ISIC Melanoma Classification Dataset	https://bit.ly/3XUqELO
	structretina	Structured Analysis of the Retina Dataset	https://bit.ly/3m0Az5b https://bit.ly/3ZjfzVJ
Satellite	amazonia1	Cloudless Scene from Amazonia 1 Satellite Dataset	https://bit.ly/3m3qKTP
	cbers4a	Scene with Clouds from CBERS-4A Satellite Dataset	https://bit.ly/3m3qKTP
	deepglobe	Forest Aerial Images for Segmentation Dataset	https://bit.ly/3Eu4Nnq
	isaid	Instance Segmentation in Aerial Images Dataset	https://bit.ly/3IpavYU

Table 2: Datasets: original resolution of the images

Domain	Dataset	Original Resolution ($W \times H$)
Aerial	condoaerial	6000 x 4000
	massachbuildings	1500 x 1500
	ships	568 x 526, 556 x 528, 550 x 570, ..., 294 x 244, 266 x 254, 238 x 232
	ufsm-flame	4000 x 3000, 254 x 254
Fauna	catsfaces	2954 x 3027, 2893 x 3016, 2418 x 2161, ..., 1024 x 837, 647 x 690, 256 x 256
	dogsfaces	678 x 796, 256 x 256
Flora	flowers	828 x 500, 819 x 500, 764 x 500, ..., 500 x 525, 500 x 507, 500 x 500
	plantpat	5184 x 3456, 4608 x 3456, 4032 x 3024, 4000 x 3000, 4000 x 2672, 3024 x 4032, 2592 x 1728
Medical	melanomaisic	6000 x 4000, 5184 x 3456, 4288 x 2848, ..., 1920 x 1080, 768 x 576, 640 x 480
	structretina	700 x 605
Satellite	amazonia1	128 x 128
	cbers4a	128 x 128
	deepglobe	256 x 256
	isaid	6661 x 6308, 6471 x 4479, 5963 x 5553, ..., 436 x 793, 395 x 590, 211 x 521

Traditionally when researchers propose a new single-image SR technique, they naturally compare their approach to other single-image SR strategies. However, it would be nice to compare single-image SR techniques to non-single-image



Figure 2: LR images from our datasets. Top row, left to right: condoaerial, massachbuildings, ships, catsfaces, dogsfaces, flowers; Bottom row, left to right: plantpat, melanomaisic, structretina, amazonia1, cbers4a, isaid

ones to perceive whether it is advantageous to consider approaches which rely on a unique image or, eventually, it is better to adopt solutions which require more than one image but not so many of them.

Thus, three of the selected techniques were designed addressing single-image SR, i.e. BlindSR, DAN, and MoESR. The other two, APA and FastGAN, are GAN-based approaches requiring a few samples indeed and were not conceived for single-image SR. Since the two latter did require more than one sample but not too many, we limited the size of the datasets to 100 LR images as mentioned in the previous section. In Section 3.4, we provide an overview of such DL strategies.

All runnings were performed using a Bull Sequana X1120 computing node of the SDumont supercomputer³, where such a node has 4 x NVIDIA Volta V100 graphics processing units (GPUs). Each run was limited to four days being considered the latest model when the execution exceeded this time.

3.4 DL techniques

In this section, we briefly describe the selected DL techniques starting with the single-image approaches. In [45], authors proposed a framework that can achieve blind image SR in a fully automated manner, while also meeting the practical scaling needs of video production. We name it here as BlindSR and such a framework is composed of three main components. The first one is a degradation-aware SR network used to generate an HR image based on a LR input image and the corresponding blur kernel. Secondly, a kernel discriminator is trained to analyse the output HR image and predict errors caused by incorrect blur kernel input. Finally, an optimisation procedure aims to recover both the degradation kernel and the HR image by minimising the predicted error using their kernel discriminator.

DAN solves the blind image SR problem via an alternating optimization algorithm which restores an HR image and estimates the corresponding blur kernel alternately [46]. Thus, these two subproblems are handled both via convolutional neural modules namely Restorer and Estimator, respectively. More specifically, the Restorer restores an HR image based on the predicted Estimator’s kernel, and the Estimator estimates a blur kernel with the help of the restored HR image.

Some blind SR techniques train a unique degradation-aware network (for multiple kernels) on external datasets like BlindSR described above [45]. But there are performance problems with these approaches. Other direction are self-supervised techniques [56] but they are usually costly and there is limited information to learn from a single image. Aiming at benefiting of the best characteristics of both types of solution, MoESR was proposed considering different experts for different degradation kernels. For every input image, the technique predicts the degradation kernel and super-resolve the LR image using the most adequate kernel-specific expert. To predict the degradation kernel, they use two components in combination. Image Sharpness Evaluator (ISE) assesses the sharpness of the images generated by the experts. These evaluations are used by the Kernel Estimation Network (KEN) to estimate the kernel and select the best pretrained expert network.

Regarding the non-single-image techniques, the greatest motivation to create APA [44] is related to the main challenge in training GANs with limited (few) data: the risk of discriminator overfitting which can lead to unstable training

³<https://sdumont.lncc.br/machine.php?pg=machine>

dynamics [57, 58]. To deal with this issue, the technique called Adaptive Pseudo Augmentation, or APA, regularises the discriminator without introducing any external augmentations or regularisation terms. Unlike previous approaches that relied on standard data augmentations [57, 58], APA leverages the generator within the GAN itself to provide the augmentation, a more natural way of regularisation of the overfitting of the discriminator. In accordance with the authors, the APA approach is simple and more adaptable to different settings and training conditions than model regularisation, without requiring manual tuning.

Other FSL solution and based on GANs is FastGAN [47]. Its authors were driven by the realisation that training GANs on high-fidelity (HR) images often necessitates a vast number of training images and large-scale GPU clusters. To address the challenge of few-shot image synthesis via GAN with minimal computing costs, FastGAN was proposed as a lightweight GAN architecture which produces high-quality results at a resolution of 1024 x 1024 pixels. Their technique involves incorporating two techniques: a skip-layer channel-wise excitation module and a self-supervised discriminator trained as a feature-encoder.

3.5 Metrics

As we have already mentioned, NIQE and the MANIQA score were the selected metrics. NIQE was calculated considering the HR images (1024 x 1024 pixels) generated by the techniques. However, according to its authors, the MANIQA model [49] is best suited for 222 x 224 pixel images. Thus, we downsampled the created HR image (1024 x 1024 pixels) to a resolution of 224 x 224 pixels in order to calculate the MANIQA score.

Note that such a degradation approach accomplished to calculate the MANIQA score was the same for all generated HR images and, therefore, there is no favouring of a certain technique in relation to the obtained value. Furthermore, we got the MANIQA score considering a subset of the datasets and HR images (1024 x 1024) and we did not notice a great difference in the scores compared to when we used the reduced images (224 x 224). Thus, we followed the authors' suggestions and considered the images in the lowest resolution (224 x 224) as input for calculating the MANIQA score.

As shown in Table 2 and as we have already pointed out, the original images of some datasets are HR ones. But there are datasets which have only original LR images and not the corresponding HR samples. In addition to that, NR-IQA metrics are more in line with the reality when we deal with a blind setting. These are the reasons to select only NR-IQA metrics for our experiment.

4 Results

In this section, we present the results of our experiment splitting the sections based on the research questions we have defined earlier.

4.1 RQ_1

4.1.1 NIQE

Table 3 presents the NIQE values in the perspective of the broader domain. In this case, we consider the mean NIQE values for all the datasets of a certain domain where the best (minimum) and worst (maximum) values, and the techniques which produced them, are shown. On the other hand, Table 4 presents a finer analysis per dataset and also considering the mean NIQE values. Recall that as lower the NIQE value, the better the perceptual quality. Fig. 3 shows all mean NIQE values considering all broader domains and datasets.

Table 3: Mean NIQE values: Broader domains

Domain	Min (Best)		Max (Worst)	
	Technique	NIQE	Technique	NIQE
Aerial	MoESR	14.648013	BlindSR	22.534419
Fauna	MoESR	14.629656	BlindSR	18.961343
Flora	MoESR	14.615975	BlindSR	21.668490
Medical	APA	14.520624	BlindSR	18.717661
Satellite	MoESR	14.385091	BlindSR	24.726333

Results show that if we consider the broader domain (Table 3), MoESR was the most outstanding approach being the best in four out of the five domains. Only in the Medical domain APA was the top technique. Moreover, BlindSR was the worst strategy with the maximum NIQE values for all domains. However, in the analysis per dataset (Table 4), APA

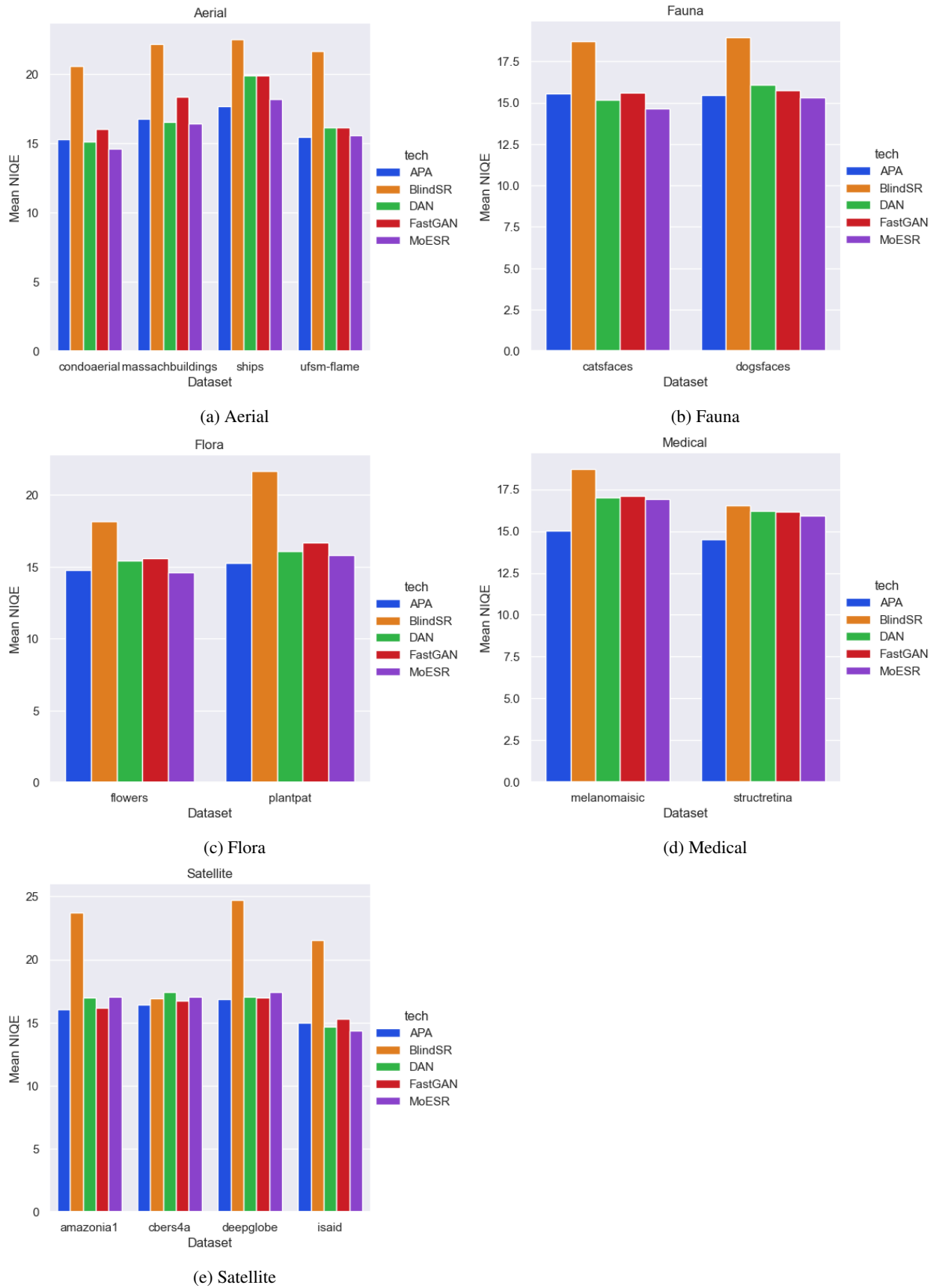


Figure 3: Mean NIQE values: All broader domains and datasets

Table 4: Mean NIQE values: Datasets

Domain	Dataset		Min (Best)	Max (Worst)
Aerial	condoaerial	MoESR	14.648013	BlindSR 20.611777
	massachbuildings	MoESR	16.427236	BlindSR 22.199742
	ships	APA	17.688239	BlindSR 22.534419
	ufsm-flame	APA	15.492423	BlindSR 21.684649
Fauna	catsfaces	MoESR	14.629656	BlindSR 18.702201
	dogsfaces	MoESR	15.314877	BlindSR 18.961343
Flora	flowers	MoESR	14.615974	BlindSR 18.174120
	plantpat	APA	15.241252	BlindSR 21.668490
Medical	melanomaisic	APA	15.025945	BlindSR 18.717661
	structretina	APA	14.520624	BlindSR 16.517888
Satellite	amazonia1	APA	16.027069	BlindSR 23.698020
	cbers4a	APA	16.398990	DAN 17.438634
	deepglobe	APA	16.863639	BlindSR 24.726333
	isaid	MoESR	14.385091	BlindSR 21.504252

was the best technique obtaining the minimum NIQE values in eight out of 14 datasets. MoESR was the best in six out of them. BlindSR was, again, the worst of all the techniques.

Since MoESR was the best in one perspective and APA was the winner in the other analysis, we performed an improvement evaluation to reach a final decision in accordance with the NIQE value. In other words, the point is not only to say that a DL technique is better than the other but how much better it is. The improvement metric, $I\%$, is calculated as follows:

$$I\% = \frac{(W - B) \times 100}{B} \quad (6)$$

where B and W are the best and worst value of the metric, respectively, comparing both techniques under the same dataset. In Table 5, we show the improvement of MoESR over APA regarding NIQE where in all datasets in this table, MoESR was superior than APA. As highlighted in **bold**, the *catsfaces* dataset was the one where MoESR got the highest improvement (6.472). In this case, $B = 14.629656$ and $W = 15.576498$. Hence, to know the APA's NIQE (W), we calculate:

$$W = B + \frac{I\%}{100} \times B. \quad (7)$$

The idea is that the improvement is the additional gain that the best approach has compared to the worst one. This is because as lower the NIQE value, the better.

Table 5: Improvement of MoESR over APA

Dataset	MoESR	APA	$I\%$
condoaerial	14.648013	15.292783	4.402
massachbuildings	16.427236	16.760828	2.031
catsfaces	14.629656	15.576498	6.472
dogsfaces	15.314877	15.444758	0.848
flowers	14.615974	14.787114	1.171
isaid	14.385091	15.01201	4.358
$\overline{I\%}$			3.214

In Table 6 is the other way around where we can see the improvement of APA over MoESR. The reasoning is the same as presented in Equations 6 and 7. Thus, the highest improvement (12.489) of APA over MoESR was obtained in the *melanomaisic* dataset. Note that this improvement of APA is almost twice the best improvement of MoESR. Furthermore, the average improvement ($\overline{I\%}$) is also higher favouring APA over MoESR. Thus, based on the NIQE metric, the best approach was APA followed by MoESR. The worst was BlindSR.

Table 6: Improvement of APA over MoESR

Dataset	APA	MoESR	I%
ships	17.688239	18.220023	3.006
ufsm-flame	15.492423	15.614556	0.788
plantpat	15.241252	15.80596	3.705
melanomaistic	15.025945	16.902496	12.489
structretina	14.520624	15.914241	9.598
amazonia1	16.027069	17.041395	6.329
cbers4a	16.39899	17.037916	3.896
deepglobe	16.863639	17.43862	3.410
$\overline{I\%}$		5.403	

4.1.2 MANIQA

In Table 7, the MANIQA scores are shown in the perspective of the broader domain while Table 8 presents the per dataset analysis. As previously, we show the mean values of the metric. Recall that as higher the MANIQA score, the better the perceptual quality. Fig. 4 shows all mean MANIQA scores considering all broader domains and datasets.

Table 7: Mean MANIQA scores: Broader domains

Domain	Max (Best)		Min (Worst)	
	Technique	MANIQA	Technique	MANIQA
Aerial	DAN	0.696858	FastGAN	0.409388
Fauna	MoESR	0.713253	FastGAN	0.515693
Flora	MoESR	0.698373	APA	0.430053
Medical	MoESR	0.614705	APA	0.432007
Satellite	DAN	0.736443	FastGAN	0.327089

Table 8: Mean MANIQA scores: Datasets

Domain	Dataset	Max (Best)	Min (Worst)
Aerial	condoaerial	MoESR	0.657257
	massachbuildings	DAN	0.696858
	ships	DAN	0.577708
	ufsm-flame	DAN	0.618042
Fauna	catsfaces	MoESR	0.713253
	dogsfaces	MoESR	0.638982
Flora	flowers	MoESR	0.698373
	plantpat	MoESR	0.606683
Medical	melanomaistic	DAN	0.542052
	structretina	MoESR	0.614705
Satellite	amazonia1	MoESR	0.579970
	cbers4a	MoESR	0.408773
	deepglobe	MoESR	0.591723
	isaid	DAN	0.736443

In the broader domain perspective, MoESR was the best (three out five top results) followed by DAN (two best positions). Unlike the NIQE metric where APA was considered the best DL technique overall, it performed poorly in accordance with the MANIQA score occupying the penultimate place (in two domains, Flora and Medical, APA was the worst approach). FastGAN was the worst of all the techniques. Again unlike the results presented in the previous section, here we have a completely agreement between the broader domain and the per dataset perspectives. Thus, considering each dataset in its own, MoESR got again the top place (nine best MANIQA scores) while DAN was the second best technique (five best MANIQA scores). Likewise, APA got the penultimate place (three worst MANIQA scores) and FastGAN was the worst of all the DL techniques.

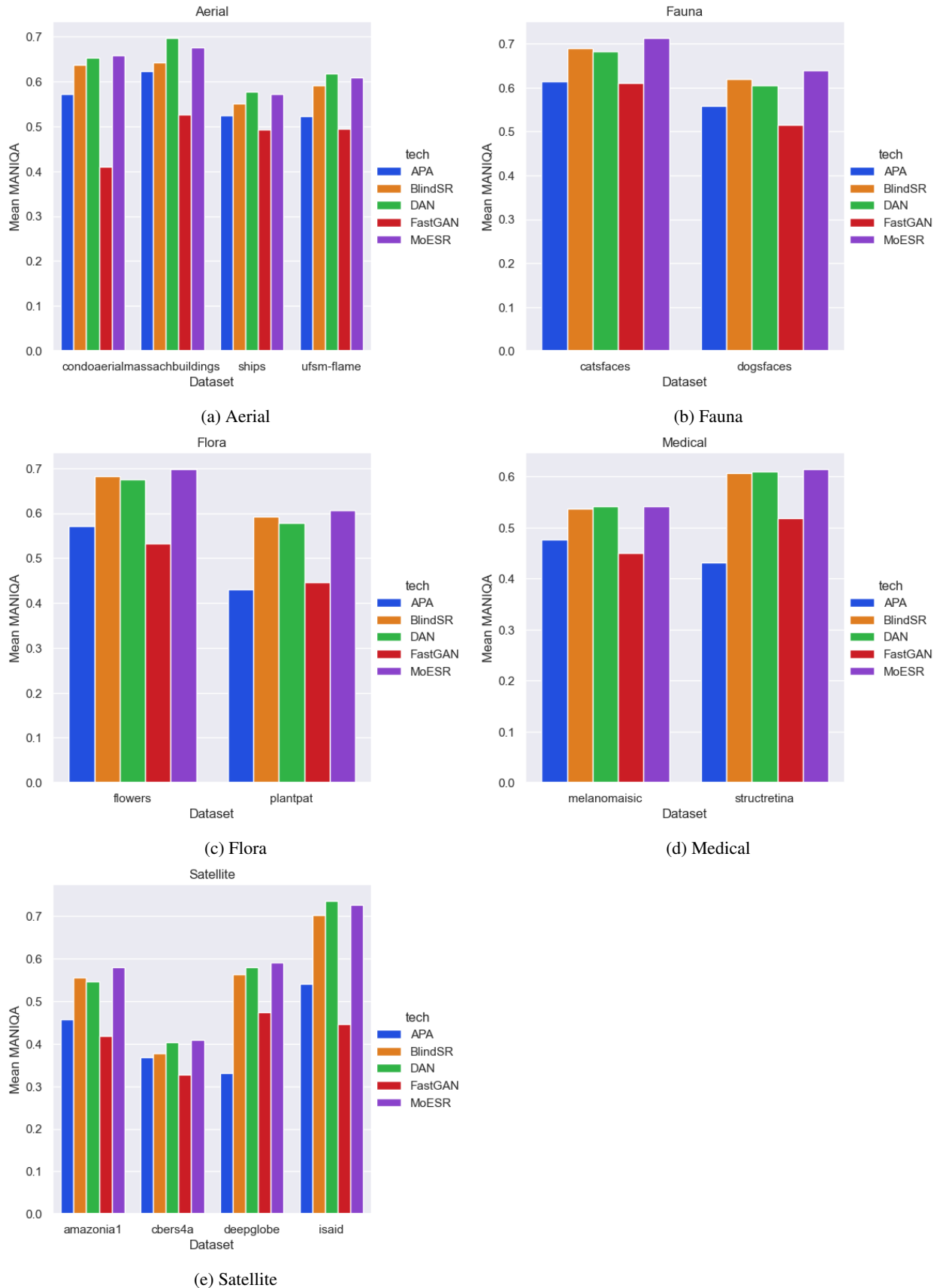


Figure 4: Mean MANIQA scores: All broader domains and datasets

Despite such an agreement, we accomplished the improvement analysis to check these results considering the two best DL models: MoESR and DAN. But, we slightly changed the way to calculate the improvement metric as shown below:

$$I\% = \frac{(B - W) \times 100}{W} \quad (8)$$

where B and W are the best and worst value of the metric, respectively, comparing both techniques under the same dataset. And now, the idea is that the improvement is the additional gain that the worst approach needs to reach the best one. This is because as higher the MANIQA score, the better. Thus, we use the following equation:

$$B = W + \frac{I\%}{100} \times W. \quad (9)$$

Table 9 presents the improvement of DAN over MoESR while Table 10 shows the opposite (MoESR over DAN). As we can see in **bold** in both tables, the highest improvement of MoESR (6.069) is almost twice the highest due to DAN (3.245). Moreover, MoESR's average improvement is also better than the DAN's average improvement. These results confirms the previous conclusions and MoESR was the best technique followed by DAN.

Table 9: Improvement of DAN over MoESR

Dataset	DAN	MoESR	I%
massachusettsbuildings	0.696858	0.674955	3.245
ships	0.577708	0.571233	1.134
ufsm-flame	0.618042	0.608577	1.555
melanomaisic	0.542052	0.541265	0.145
isaid	0.736443	0.72679	1.328
$\overline{I\%}$			1.481

Table 10: Improvement of MoESR over DAN

Dataset	MoESR	DAN	I%
condoaerial	0.657257	0.653125	0.633
catsfaces	0.713253	0.681594	4.645
dogsfaces	0.638982	0.605406	5.546
flowers	0.698373	0.674927	3.474
plantpat	0.606683	0.578225	4.922
structretina	0.614705	0.609501	0.854
amazonia1	0.57997	0.546786	6.069
cbers4a	0.408773	0.403834	1.223
deepglobe	0.591723	0.580666	1.904
$\overline{I\%}$			3.252

Considering both metrics, NIQE and MANIQA score, we can state that MoESR was the most outstanding approach. It presented a consistent performance under NIQE, being the second best technique, and, as we have just said, it got the top place based on the MANIQA score. Note that we saw contradictory performances regarding APA where it was the best strategy evaluated via NIQE and almost the worst approach, if we take into account the MANIQA score.

4.2 RQ.2

Question **RQ.2** is about the similarity of behaviours between the two best approaches according to the MANIQA score: MoESR and DAN. Here, our intention is to see whether the two best models “agree” in terms of the HR images they create. Thus, we took the 10 images with the best MANIQA scores from both techniques, for each dataset, and generated two sets $High_M$ and $High_D$, meaning the scores of the images from MoESR and DAN, respectively. Hence, we just calculated the cardinality of a new set (C_B) derived by the intersection between the previous two sets:

$$|C_B| = |High_M \cap High_D|. \quad (10)$$

We also did the same and calculated the cardinality of the set of non-common elements, N_B , such that:

$$|N_B| = \frac{|High_M \cup High_D| - |High_M \cap High_D|}{2}. \quad (11)$$

For instance, for the *condoaerial* dataset, $|C_B(\text{condoaerial})| = 7$. This implies that seven out of the 10 images with the highest MANIQA scores are common to MoESR and DAN, and hence there is an agreement between both techniques regarding these images. Thus, $|N_B(\text{condoaerial})| = 3$, representing that three out of the 10 images are not common showing disagreement. The average value of the cardinalities of all common sets is $\overline{C_B(\text{all})} = 7.36$ while for the non-common case is $\overline{N_B(\text{all})} = 2.64$.

We did the same with the 10 images with lowest scores and created the sets Low_M and Low_D due to MoESR and DAN, respectively. Likewise, we calculated the cardinality of C_W and N_W for each dataset, just replacing the high sets by the low ones in the Equations 10 and 11. For example, for the *amazonia1* dataset, $|C_W(\text{amazonia1})| = 6$ and $|N_W(\text{amazonia1})| = 4$, meaning that six images with the lowest scores are common and four are not common. The average value of the cardinalities of all common sets is $\overline{C_W(\text{all})} = 7.5$ while for the non-common case is $\overline{N_W(\text{all})} = 2.5$.

Finally, we obtained the Kendall Rank Correlation Coefficient (Kendall's τ coefficient) for two situations. The first case is considering C_B and C_W and the second situation is based on N_B and N_W . In both cases, $\tau = 0.306912$ showing a good correlation between each pair of variables. Fig. 5 shows the correlation in detail.

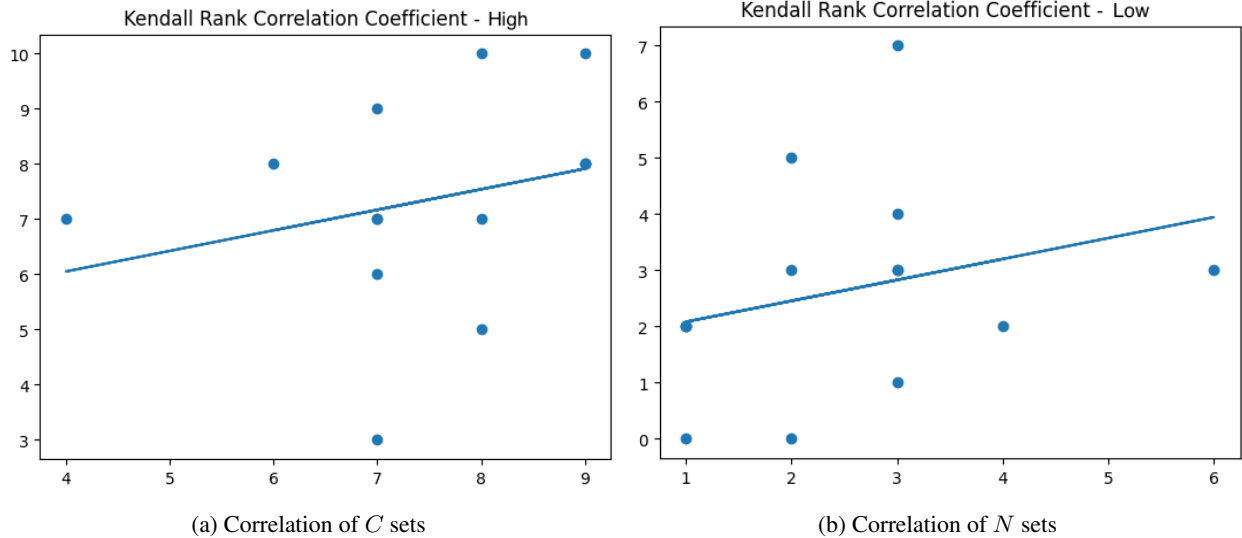


Figure 5: Kendall Rank Correlation Coefficient: results

The interpretation of these results is that the images detected as having the best, as well as the worst, perceptual qualities, based on the MANIQA scores, are somewhat "common" to both techniques. Hence, we can conclude that both approaches present a similar behaviour. It is important to emphasise that the relevance of this analysis is to realise whether the two best approaches generate HR images with better or worse perception qualities in a relatively uniform manner, taking the LR images as input.

5 Discussion

We start this section by stressing some points based on a visual analysis. Fig. 6 shows the LR image and a piece of the corresponding HR image generated by the three single-image blind SR techniques. The top HR image generated by DAN, based on an LR image of the *isaid* Satellite dataset, is the one with the highest MANIQA score (0.850084) of all images. We clearly see that the roof divisions of the building appear more vivid in the image created by DAN. MoESR's image appears blurred while BlindSR's image seems to present something like a salt-and-pepper noise.

On the other hand, the bottom HR image created by BlindSR is the one with the lowest MANIQA score (0.240234) of all images. The LR image is from the *cbers4a* Satellite dataset where the scene presents water and land. This is a

cloudy scene obtained by the CBERS-4A satellite and it is interesting to realise that such bright images from `cbers4a` in general produced the lowest MANIQA scores (see Fig. 4e).



Figure 6: Visual analysis: highest and lowest MANIQA scores

Other LR images and the corresponding piece of HR images created by the three single-image blind SR models are presented in Fig. 7. MoESR produced the highest MANIQA score for the top images (`condoaerial`, `flowers`, `melanomaistic`, `amazonia1`) while DAN produced the highest score for the bottom one (`deepglobe`).

Since APA and FastGAN are GAN-based non-single image techniques, some known issues of GANs appeared here. In order to use APA in a custom dataset, three phases are required: prepare the dataset, training, and inference for generating images. As usual, the training is the more demanded step and APA indeed exceeded the limit we set up (four days) not finishing the training. We considered its latest model for inference. We used 4 x NVIDIA Volta V100 GPUs and the datasets are very small (100 samples). It is important to mention that other DL techniques demanded only one out of the four GPUs and the limit was enough for them. Thus, APA is a very “heavy” model. Furthermore, some HR images were flipped and others upside down compared to the source LR images. There are even cases where the images were not indeed generated (it is likely that the images are basically noise).

Fig. 8 shows these cases where we have the LR image and the corresponding APA’s HR image. Note that we downsampled the APA images to 128 x 128 pixels for this figure to compare to the LR images. Moreover, the `deepglobe` image is here just to show a sample of the dataset since APA’s output seems to be basically noise.

As for FastGAN, the required phases to use it are training and inference, and its training is considerably faster/lighter than APA. But both FastGAN and APA presented a very known problem related to GANs: mode collapse [59]. It happens when the generator model produces a not very significant set of images that fail to capture the full diversity of the real data distribution. Thus, the fake created samples are quite similar or even identical. In Fig. 9, we see some images from FastGAN where mode collapse occurs. Again, we downgraded the HR images for better presentation.

Based on the MANIQA scores (Section 4.1.2), APA and FastGAN were the worst techniques. Thus, we can conclude based on the results of our experiment that, for blind image SR, single-image and non-GAN-based approaches are the best way to go.

Considering the best two DL techniques in accordance with the MANIQA score, we may say that the HR images created by MoESR are sharper than the ones of DAN. Fig. 10 presents the measures of the maximum overall contrast of the images with the highest MANIQA scores taking into account both techniques and the 14 datasets. For instance, for the `amazonia1` dataset, the image derived by MoESR has higher MANIQA score than the one of DAN and, thus, we considered the former and the corresponding DAN’s image. As for `isaid`, DAN’s image got higher MANIQA score

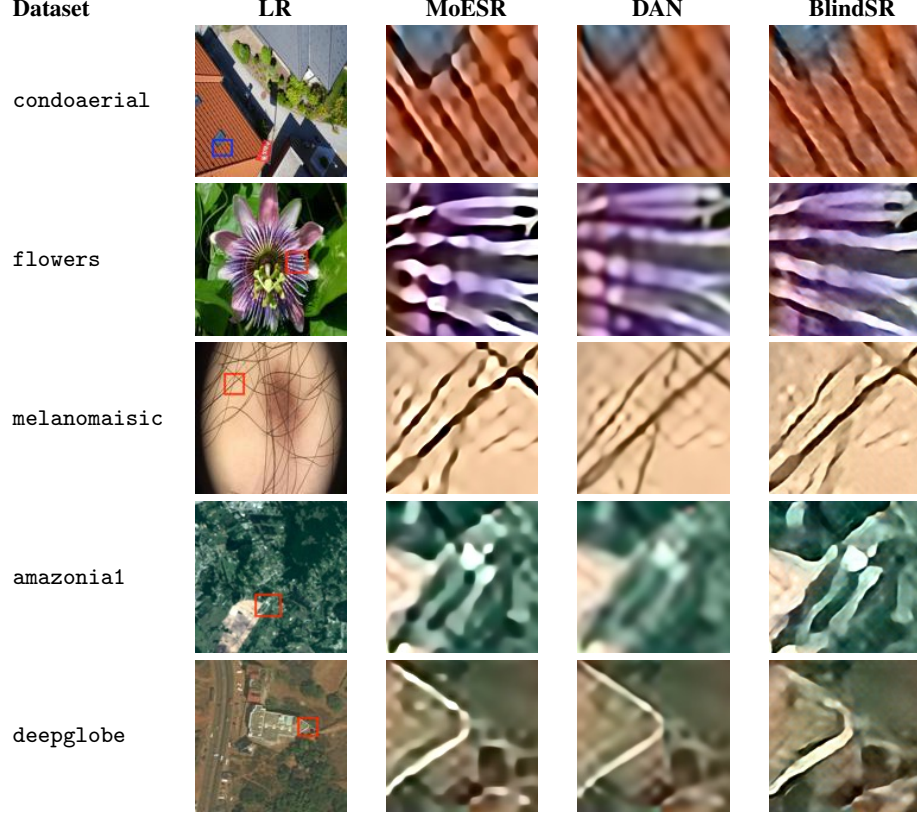


Figure 7: Other created HR images by the single-image blind SR approaches

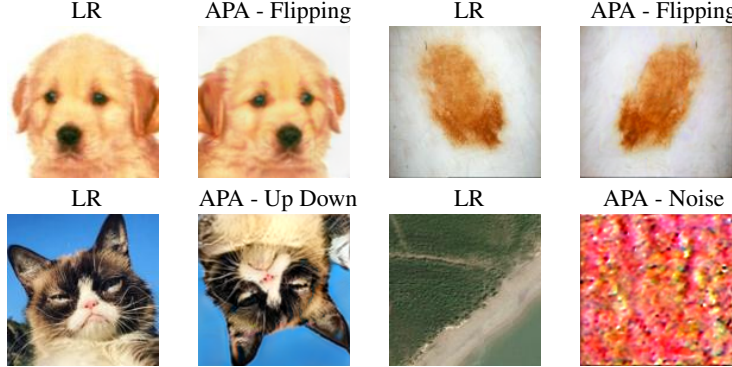


Figure 8: Some issues presented by APA. Top row, left to right: dogsfaces, melanomaisic; Bottom row, left to right: catsfaces, deepglobe

and thus this image and the corresponding MoESR’s image were analysed. Fig. 11 follows the same reasoning but now the images are the ones with the lowest MANIQA scores.

Since the higher the maximum overall contrast the sharper the image, we can realise that the images of MoESR are sharper than the ones of DAN. But, note that perceptual quality is not necessarily the same thing as sharpness. An image with higher contrast does not imply that it has a better perceptual quality than one with lower contrast.

A possible explanation for the images created by MoESR being sharper than DAN’s images, and sometimes present oversharpening, is the combination of the performances of ISE and KEN. The ISE component is trained to detect blurry or oversharpened regions and predicts errors from the ground-truth image. Since KEN uses the sharpness measures from ISE to estimate the kernel and select the best pretrained model, misleading evaluations of sharpness by ISE may compromise the decision made by the KEN component.



Figure 9: Mode collapse in FastGAN: condoaerial

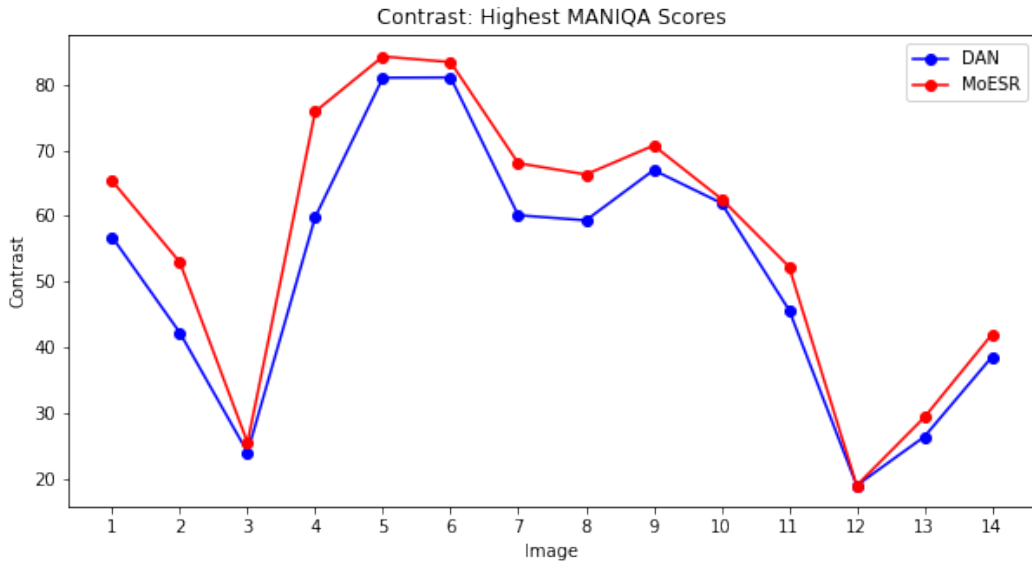


Figure 10: Highest MANIQA scores: Contrast

On the other hand, HR images generated by DAN are generally blurry which might lead to a poor perceptual quality. In DAN, the kernel is initialised by Dirac function, and it is also reshaped and then reduced by principal component analysis (PCA) [60]. The kernel is reduced by PCA and thus the Estimator only needs to estimate the PCA result of the blur kernel. There is naturally loss of information when using PCA for dimensionality reduction, and recent evaluations show that PCA results are not as reliable and robust as it is usually assumed to be [61]. This is a possible explanation for this issue related to DAN.

As mentioned in Section 4, there is not an agreement between the ranking of best and worst techniques considering a classical metric (NIQE) and a DNN-based one (MANIQA score). While APA presented the better performance under NIQE, it is almost the worst solution according to the MANIQA score. Thus, we believe that relying on a more recent NR-IQA metric, like the MANIQA score and which presented quite superior performance [41] than traditional metrics, is more advisable.

Notice that we do not have the mean opinion scores (MOSs) of the HR images as we do not submit them for observers to assign it. But, looking at the HR images generated by all DL techniques for all sets (see the datasets repository of this research), it is not difficult to see that the perception quality of the images as a whole needs to improve. Note that in MoESR and DAN, the generation of the HR images had to be done in two stages, using the 2x and 4x scaling factors in sequence. In general, there are several blurred images and others with oversharpening. Despite the sophistication of the evaluated DNNs, we believe that new approaches, addressing larger scaling factors, are necessary for the future.

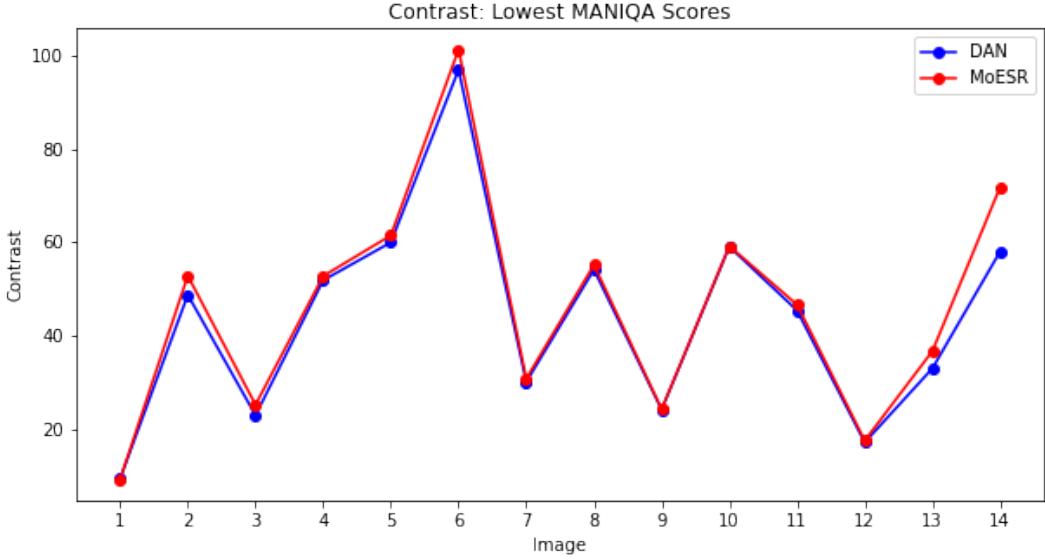


Figure 11: Lowest MANIQA scores: Contrast

6 Conclusions

Given the significant number of DL techniques/DNNs which are created on a daily basis, it is relevant to perform independent and unbiased controlled experiments to suggest the most suitable approaches for professionals. This article is in line with this reasoning, where we presented an large scaling factor (8x) experiment which evaluated recent DL techniques tailored for blind image SR: APA, BlindSR, DAN, FastGAN, and MoESR. Some of the techniques were designed for single-image while others for non-single-image blind SR. In addition to selecting a larger scaling factor, another difference in this study is that we showed a more detailed analysis of the results, also focusing on explaining in depth the behaviours of the approaches. Mostly based on publicly released sources of images, we adapted and created 14 small (100 samples) LR images datasets from five different broader domains to provide a significant range of distinct images to the techniques. We also considered two NR-IQA metrics, the classical NIQE and the DNN-based MANIQA score.

Results show that the MoESR model was the most outstanding approach followed by DAN. GAN-based approaches presented classical issues such as mode collapse and noise, in some cases. The outcomes of our experiment suggest that single-image and non-GAN-based techniques are more promising for blind image SR, although such a conclusion needs more experimentation to be completely confirmed. By visually inspecting the HR images created by the techniques, we may state that, despite the remarkable solutions, new strategies are required for larger scaling factor requirements.

As future directions, we firstly intend to carry out even higher scaling factor experiments, such as 16x. We will also increase not only the amount of blind image SR approaches to assess but also the number of datasets to get more evidences about the conclusions we have made. Other recent NR-IQA metrics will also be considered in these new controlled experiments.

Acknowledgements

This research was developed within the project *Classificação de imagens via redes neurais profundas e grandes bases de dados para aplicações aeroespaciais* (Image classification via Deep neural networks and large databases for aeroSpace applications - **IDeepS**). The **IDeepS** (<https://github.com/vsantjr/IDeepS>) project is supported by the *Laboratório Nacional de Computação Científica* (LNCC/MCTI, Brazil) via resources of the SDumont supercomputer (<http://sdumont.lncc.br>).

References

- [1] K. Yamashita and K. Markov. Medical image enhancement using super resolution methods. In Valeria V. Krzhizhanovskaya, Gábor Závodszky, Michael H. Lees, Jack J. Dongarra, Peter M. A. Sloot, Sérgio Brissos, and João Teixeira, editors, *Computational Science – ICCS 2020*, pages 496–508, Cham, 2020. Springer International Publishing.
- [2] Y. Huang, L. Shao, and A. F. Frangi. Simultaneous super-resolution and cross-modality synthesis of 3d medical images using weakly-supervised joint convolutional sparse coding. In *2017 IEEE Conference on Computer Vision and Pattern Recognition (CVPR)*, pages 5787–5796, Los Alamitos, CA, USA, jul 2017. IEEE Computer Society.
- [3] W. Ahmad, H. Ali, Z. Shah, and S. Azmat. A new generative adversarial network for medical images super resolution. *Scientific Reports*, 12:9533, 2022. <https://doi.org/10.1038/s41598-022-13658-4>.
- [4] R. Gupta, A. Sharma, and A. Kumar. Super-resolution using gans for medical imaging. *Procedia Computer Science*, 173:28–35, 2020. International Conference on Smart Sustainable Intelligent Computing and Applications under ICITETM2020.
- [5] J. M. Liborio, C. Melo, and M. Silva. Internet video delivery improved by super-resolution with gan. *Future Internet*, 14(12), 2022.
- [6] H. Yeo, Y. Jung, J. Kim, J. Shin, and D. Han. Neural adaptive content-aware internet video delivery. In *Proceedings of the 13th USENIX Conference on Operating Systems Design and Implementation*, OSDI’18, pages 645–661, USA, 2018. USENIX Association.
- [7] H. Yeo, S. Do, and D. Han. How will deep learning change internet video delivery? In *HotNets-XVI: Proceedings of the 16th ACM Workshop on Hot Topics in Networks*, pages 57–64, 2017.
- [8] P. Rasti, T. Uiboupin, S. Escalera, and G. Anbarjafari. Convolutional neural network super resolution for face recognition in surveillance monitoring. In Francisco José Perales and Josef Kittler, editors, *Articulated Motion and Deformable Objects*, pages 175–184, Cham, 2016. Springer International Publishing.
- [9] E. Zhou, H. Fan, Z. Cao, Y. Jiang, and Q. Yin. Learning face hallucination in the wild. *Proceedings of the AAAI Conference on Artificial Intelligence*, 29(1), Mar. 2015.
- [10] S. Zhu, S. Liu, C. C. Loy, and X. Tang. Deep cascaded bi-network for face hallucination. In Bastian Leibe, Jiri Matas, Nicu Sebe, and Max Welling, editors, *Computer Vision – ECCV 2016*, pages 614–630, Cham, 2016. Springer International Publishing.
- [11] P. Wang, B. Bayram, and E. Sertel. A comprehensive review on deep learning based remote sensing image super-resolution methods. *Earth-Science Reviews*, 232:104110, 2022.
- [12] K. Jiang, Z. Wang, P. Yi, G. Wang, T. Lu, and J. Jiang. Edge-enhanced gan for remote sensing image superresolution. *IEEE Transactions on Geoscience and Remote Sensing*, 57(8):5799–5812, 2019.
- [13] K. Jiang, Z. Wang, P. Yi, J. Jiang, J. Xiao, and Y. Yao. Deep distillation recursive network for remote sensing imagery super-resolution. *Remote Sensing*, 10(11), 2018.
- [14] Y. Xu, W. Luo, A. Hu, Z. Xie, X. Xie, and L. Tao. Te-sagan: An improved generative adversarial network for remote sensing super-resolution images. *Remote Sensing*, 14(10), 2022.
- [15] B. Niu, W. Wen, W. Ren, X. Zhang, L. Yang, S. Wang, K. Zhang, X. Cao, and H. Shen. Single image super-resolution via a holistic attention network. In Andrea Vedaldi, Horst Bischof, Thomas Brox, and Jan-Michael Frahm, editors, *Computer Vision – ECCV 2020*, pages 191–207, Cham, 2020. Springer International Publishing.
- [16] J. Zhang, T. Xu, J. Li, S. Jiang, and Y. Zhang. Single-image super resolution of remote sensing images with real-world degradation modeling. *Remote Sensing*, 14(12), 2022.
- [17] Z. Wang, J. Chen, and S. C. H. Hoi. Deep learning for image super-resolution: A survey. *IEEE Transactions on Pattern Analysis and Machine Intelligence*, 43(10):3365–3387, 2021.
- [18] C. E. Duchon. Lanczos filtering in one and two dimensions. *Journal of Applied Meteorology and Climatology*, 18(8):1016 – 1022, 1979.
- [19] J. Sun, Z. Xu, and H.-Y. Shum. Image super-resolution using gradient profile prior. In *2008 IEEE Conference on Computer Vision and Pattern Recognition*, pages 1–8, 2008.
- [20] Z. Xiong, X. Sun, and F. Wu. Robust web image/video super-resolution. *IEEE Transactions on Image Processing*, 19(8):2017–2028, 2010.
- [21] J. Egger, A. Pepe, C. Gsaxner, Y. Jin, J. Li, and R. Kern. Deep learning-a first meta-survey of selected reviews across scientific disciplines, their commonalities, challenges and research impact. *PeerJ Computer science*, 7, 2021. © 2021 Egger et al.

- [22] C. Dong, C. C. Loy, K. He, and X. Tang. Learning a deep convolutional network for image super-resolution. In David Fleet, Tomas Pajdla, Bernt Schiele, and Tinne Tuytelaars, editors, *Computer Vision – ECCV 2014*, pages 184–199, Cham, 2014. Springer International Publishing.
- [23] J. Kim, J. Lee, and K. Lee. Accurate image super-resolution using very deep convolutional networks. In *2016 IEEE Conference on Computer Vision and Pattern Recognition (CVPR)*, pages 1646–1654, Los Alamitos, CA, USA, jun 2016. IEEE Computer Society.
- [24] B. Lim, S. Son, H. Kim, S. Nah, and K. M. Lee. Enhanced deep residual networks for single image super-resolution. In *2017 IEEE Conference on Computer Vision and Pattern Recognition Workshops (CVPRW)*, pages 1132–1140, 2017.
- [25] C. Ledig, L. Theis, F. Huszar, J. Caballero, A. Cunningham, A. Acosta, A. Aitken, A. Tejani, J. Totz, Z. Wang, and W. Shi. Photo-realistic single image super-resolution using a generative adversarial network. In *Proceedings of the IEEE Conference on Computer Vision and Pattern Recognition (CVPR)*, July 2017.
- [26] X. Wang, K. Yu, S. Wu, J. Gu, Y. Liu, C. Dong, Y. Qiao, and C. Change Loy. Esrgan: Enhanced super-resolution generative adversarial networks. In *Proceedings of the European Conference on Computer Vision (ECCV) Workshops*, September 2018.
- [27] Y. Zhang, K. Li, K. Li, L. Wang, B. Zhong, and Y. Fu. Image super-resolution using very deep residual channel attention networks. In *Proceedings of the European Conference on Computer Vision (ECCV)*, September 2018.
- [28] X. Cheng, X. Li, J. Yang, and Y. Tai. Sesr: Single image super resolution with recursive squeeze and excitation networks. In *2018 24th International Conference on Pattern Recognition (ICPR)*, pages 147–152, 2018.
- [29] A. Bulat, J. Yang, and G. Tzimiropoulos. To learn image super-resolution, use a gan to learn how to do image degradation first. In Vittorio Ferrari, Martial Hebert, Cristian Sminchisescu, and Yair Weiss, editors, *Computer Vision – ECCV 2018*, pages 187–202, Cham, 2018. Springer International Publishing.
- [30] J. Gu, H. Lu, W. Zuo, and C. Dong. Blind super-resolution with iterative kernel correction. In *2019 IEEE/CVF Conference on Computer Vision and Pattern Recognition (CVPR)*, pages 1604–1613, Los Alamitos, CA, USA, jun 2019. IEEE Computer Society.
- [31] Z. Yue, Q. Zhao, J. Xie, L. Zhang, D. Meng, and K. K. Wong. Blind image super-resolution with elaborate degradation modeling on noise and kernel. In *2022 IEEE/CVF Conference on Computer Vision and Pattern Recognition (CVPR)*, pages 2118–2128, Los Alamitos, CA, USA, jun 2022. IEEE Computer Society.
- [32] D. Martin, C. Fowlkes, D. Tal, and J. Malik. A database of human segmented natural images and its application to evaluating segmentation algorithms and measuring ecological statistics. In *Proceedings Eighth IEEE International Conference on Computer Vision. ICCV 2001*, volume 2, pages 416–423 vol.2, 2001.
- [33] P. Arbeláez, M. Maire, C. Fowlkes, and J. Malik. Contour detection and hierarchical image segmentation. *IEEE Transactions on Pattern Analysis and Machine Intelligence*, 33(5):898–916, 2011.
- [34] E. Agustsson and R. Timofte. Ntire 2017 challenge on single image super-resolution: Dataset and study. In *2017 IEEE Conference on Computer Vision and Pattern Recognition Workshops (CVPRW)*, pages 1122–1131, 2017.
- [35] Y. Blau, R. Mechrez, R. Timofte, T. Michaeli, and L. Zelnik-Manor. The 2018 pirm challenge on perceptual image super-resolution. In Laura Leal-Taixé and Stefan Roth, editors, *Computer Vision – ECCV 2018 Workshops*, pages 334–355, Cham, 2019. Springer International Publishing.
- [36] M. Bevilacqua, A. Roumy, C. Guillemot, and M. A. Morel. Low-complexity single-image super-resolution based on nonnegative neighbor embedding. In R. Bowden, J. Collomosse, and K. Mikolajczyk, editors, *Proceedings of the British Machine Vision Conference*, pages 1–10, Durham, UK, 2012. BMVA Press.
- [37] R. Zeyde, M. Elad, and M. Protter. On single image scale-up using sparse-representations. In Jean-Daniel Boissonnat, Patrick Chenin, Albert Cohen, Christian Gout, Tom Lyche, Marie-Laurence Mazure, and Larry Schumaker, editors, *Curves and Surfaces*, pages 711–730, Berlin, Heidelberg, 2012. Springer Berlin Heidelberg.
- [38] J.-B. Huang, A. Singh, and N. Ahuja. Single image super-resolution from transformed self-exemplars. In *2015 IEEE Conference on Computer Vision and Pattern Recognition (CVPR)*, pages 5197–5206, 2015.
- [39] Z. Yuan, C. Tang, A. Yang, W. Huang, and W. Chen. Few-shot remote sensing image scene classification based on metric learning and local descriptors. *Remote Sensing*, 15(3), 2023.
- [40] M. Haris, G. Shakhnarovich, and N. Ukita. Deep back-projection networks for super-resolution. In *2018 IEEE/CVF Conference on Computer Vision and Pattern Recognition (CVPR)*, pages 1664–1673, Los Alamitos, CA, USA, jun 2018. IEEE Computer Society.

- [41] J. Gu, H. Cai, C. Dong, J. S. Ren, R. Timofte, Y. Gong, S. Lao, S. Shi, J. Wang, S. Yang, T. Wu, W. Xia, Y. Yang, M. Cao, C. Heng, L. Fu, R. Zhang, Y. Zhang, H. Wang, H. Song, J. Wang, H. Fan, X. Hou, M. Sun, M. Li, K. Zhao, K. Yuan, Z. Kong, M. Wu, C. Zheng, M. V. Conde, M. Burchi, L. Feng, T. Zhang, Y. Li, J. Xu, H. Wang, Y. Liao, J. Li, K. Xu, T. Sun, Y. Xiong, A. Keshari, K. Komal, S. Thakur, V. Jakhetiya, B. N. Subudhi, H. Yang, H. Chang, Z. Huang, W. Chen, S. Kuo, S. Dutta, S. Das, N. A. Shah, and A. Tiwari. Ntire 2022 challenge on perceptual image quality assessment. In *2022 IEEE/CVF Conference on Computer Vision and Pattern Recognition Workshops (CVPRW)*, pages 950–966, Los Alamitos, CA, USA, jun 2022. IEEE Computer Society.
- [42] Z. Wang, A. C. Bovik, H. R. Sheikh, and E. P. Simoncelli. Image quality assessment: from error visibility to structural similarity. *IEEE Transactions on Image Processing*, 13(4):600–612, 2004.
- [43] A. Mittal, R. Soundararajan, and A. C. Bovik. Making a “completely blind” image quality analyzer. *IEEE Signal Processing Letters*, 20(3):209–212, 2013.
- [44] L. Jiang, B. Dai, W. Wu, and C. C. Loy. Deceive d: Adaptive pseudo augmentation for gan training with limited data. In M. Ranzato, A. Beygelzimer, Y. Dauphin, P.S. Liang, and J. Wortman Vaughan, editors, *Advances in Neural Information Processing Systems*, volume 34, pages 21655–21667. Curran Associates, Inc., 2021.
- [45] V. Cornillère, A. Djelouah, W. Yifan, O. Sorkine-Hornung, and C. Schroers. Blind image super-resolution with spatially variant degradations. *ACM Trans. Graph.*, 38(6), nov 2019.
- [46] Z. Luo, Y. Huang, S. Li, L. Wang, and T. Tan. Unfolding the alternating optimization for blind super resolution. In H. Larochelle, M. Ranzato, R. Hadsell, M.F. Balcan, and H. Lin, editors, *Advances in Neural Information Processing Systems*, volume 33, pages 5632–5643. Curran Associates, Inc., 2020.
- [47] B. Liu, Y. Zhu, K. Song, and A. Elgammal. Towards faster and stabilized {gan} training for high-fidelity few-shot image synthesis. In *International Conference on Learning Representations*, 2021.
- [48] M. Emad, M. Peemen, and H. Corporaal. Moesr: Blind super-resolution using kernel-aware mixture of experts. In *2022 IEEE/CVF Winter Conference on Applications of Computer Vision (WACV)*, pages 4009–4018, 2022.
- [49] S. Yang, T. Wu, S. Shi, S. Lao, Y. Gong, M. Cao, J. Wang, and Y. Yang. Maniq: Multi-dimension attention network for no-reference image quality assessment, 2022.
- [50] K. Zhang, W. Zuo, and L. Zhang. Learning a single convolutional super-resolution network for multiple degradations. In *IEEE Conference on Computer Vision and Pattern Recognition*, pages 3262–3271, 2018.
- [51] M. Anderson, T. Adali, and X.-L. Li. Joint blind source separation with multivariate gaussian model: Algorithms and performance analysis. *IEEE Transactions on Signal Processing*, 60(4):1672–1683, 2012.
- [52] J. Gu, Y. Shen, and B. Zhou. Image processing using multi-code gan prior. In *IEEE/CVF Conference on Computer Vision and Pattern Recognition (CVPR)*, pages 3012—3021, June 2020.
- [53] A. Dosovitskiy, L. Beyer, A. Kolesnikov, D. Weissenborn, X. Zhai, T. Unterthiner, M. Dehghani, M. Minderer, G. Heigold, S. Gelly, J. Uszkoreit, and N. Houlsby. An image is worth 16x16 words: Transformers for image recognition at scale. In *International Conference on Learning Representations*, 2021.
- [54] Y. Wang, Q. Yao, J. T. Kwok, and L. M. Ni. Generalizing from a few examples: A survey on few-shot learning. *ACM Comput. Surv.*, 53(3), jun 2020.
- [55] M. Irani A. Shocher, N. Cohen. ”Zero-Shot” super-resolution using deep internal learning. In *The IEEE Conference on Computer Vision and Pattern Recognition (CVPR)*, June 2018.
- [56] S. Bell-Kligler, A. Shocher, and M. Irani. *Blind Super-Resolution Kernel Estimation Using an Internal-GAN*. Curran Associates Inc., Red Hook, NY, USA, 2019.
- [57] T. Karras, M. Aittala, J. Hellsten, S. Laine, J. Lehtinen, and T. Aila. Training generative adversarial networks with limited data. In *Proceedings of the 34th International Conference on Neural Information Processing Systems*, NIPS’20, Red Hook, NY, USA, 2020. Curran Associates Inc.
- [58] S. Zhao, Z. Liu, J. Lin, J.-Y. Zhu, and S. Han. Differentiable augmentation for data-efficient gan training. In *Proceedings of the 34th International Conference on Neural Information Processing Systems*, NIPS’20, Red Hook, NY, USA, 2020. Curran Associates Inc.
- [59] A. Srivastava, L. Valkov, C. Russell, M. U. Gutmann, and C. Sutton. Veegan: Reducing mode collapse in gans using implicit variational learning. *Neural Information Processing Systems*, 2017.
- [60] A. Mackiewicz and W. Ratajczak. Principal components analysis (pca). *Computers & Geosciences*, 19(3):303–342, 1993.
- [61] E. Elhaik. Principal component analyses (pca)-based findings in population genetic studies are highly biased and must be reevaluated. *Scientific Reports*, 12(14683), 2022. <https://doi.org/10.1038/s41598-022-14395-4>.